



Cite this: *Polym. Chem.*, 2019, **10**, 2527

## Ferrocene-containing amphiphilic polynorbornenes as biocompatible drug carriers†

Guirong Qiu,<sup>a</sup> Xiong Liu,<sup>a,b</sup> Binrong Wang,<sup>c</sup> Haibin Gu \*<sup>a,b</sup> and Weixiang Wang\*<sup>c</sup>

Redox-stimuli responsive amphiphilic copolymers have recently emerged as promising drug carrier systems with controllable drug release. Herein, we first reported the synthesis of two well-defined redox-stimuli responsive ferrocene-containing polymers, amphiphilic diblock copolymer **PN(Fc-b-TEG)** and random copolymer **PN(Fc-r-TEG)**, via ring-opening metathesis polymerization (ROMP), and compared their properties as drug carriers. Results showed that both of the obtained copolymers could self-assemble into globular nanoscale core-shell micelles in aqueous solution and showed tunable redox responses. The copolymer micelles were used to entrap the hydrophobic dye Nile red (NR) or anticancer drug doxorubicin (DOX). The DOX encapsulation efficiency of **PN(Fc-b-TEG)** is 66.7% which is higher than that of **PN(Fc-r-TEG)** (21.1%) under the same conditions. Meanwhile, the DOX-loaded micelles exhibited oxidation-controlled drug release, and the release rate could be mediated by the concentration of oxidants. Cell counting kit (CCK) assay and model organism zebrafish embryo studies were further performed to disclose the biocompatibility and safety of the copolymer micelles, and the results showed that the copolymers had excellent biocompatibility. The neoteric ferrocene-containing copolymer carriers with reversible redox-response are anticipated to have potential in targeted drug delivery systems for cancer therapy.

Received 1st March 2019,  
Accepted 4th April 2019

DOI: 10.1039/c9py00332k  
rsc.li/polymers

### 1. Introduction

Cancer, the most common category of malignant tumors, is one of the manifest causes of death in the world today and seriously threatens human health.<sup>1</sup> Up to now, surgical resection is the optimal therapy for malignant tumors at early stages, but the recurrence rate of tumors is still high after surgery.<sup>1–5</sup> Chemotherapy as the main treatment for tumor recurrence, especially for tumors at the middle and late stages, has been widely applied in clinical applications.<sup>6–8</sup> However, it causes undesirable side-effects in human normal tissues during therapy due to the wide biodistribution of chemotherapeutic agents and their lack of specificity for cancer cells.<sup>3</sup> As a result, this drawback restricts the use of cytotoxic small molecules including paclitaxel (PTX), vincristine, cisplatin, gemcitabine and doxorubicin (DOX), which are known as anticancer drugs to inhibit the highly proliferative behavior of cancer cells.<sup>9</sup>

To overcome this drawback, one promising route to improve treatment is the use of “smart drug carriers” including liposomes, microspheres and micelles, which can encapsulate toxic drugs into the core of the carriers during transport, and release them under specific external stimulation, such as pH, light, temperature, ultrasound, enzymes, electricity, solvent or redox stimuli, at the target tumor site.<sup>3,10–17</sup> Among them, redox-responsive drug carrier systems (DCSs) have attracted growing research efforts owing to the high involvement of redox reactions in many important biological processes including cellular respiration and apoptosis.<sup>18–21</sup> For example, Liu *et al.* developed DCSs based on redox-responsive supramolecular micelles, formed by anthraquinone (AQ) and cyclodextrins with disulfide bonds, for targeted imaging and drug delivery to tumors.<sup>22</sup>

Ferrocene (Fc), which is a redox-responsive organometallic compound with a typical sandwich structure of [Fe ( $\eta^5$ -C<sub>5</sub>H<sub>5</sub>)<sub>2</sub>] and which possesses reversible redox activity and stability, has been widely used as a smart building unit to construct various redox-stimuli-responsive polymer carriers.<sup>23–34</sup> For example, Xu *et al.*<sup>35</sup> constructed a redox-responsive Fc-containing amphiphilic block copolymer by using the atom transfer radical polymerization (ATRP) technique with poly(*N*-acryloylmorpholine) (PACMO) as hydrophilic blocks and poly(2-acryloyloxyethyl ferrocenecarboxylate) (PAEFC) as hydrophobic blocks. The resulting copolymer was used to entrap the anticancer drug PTX and exhibited oxidation-controlled drug release behavior, and the release rate

<sup>a</sup>Key Laboratory of Leather Chemistry and Engineering of Ministry of Education, Sichuan University, Chengdu 610065, China. E-mail: guhaibinkong@126.com

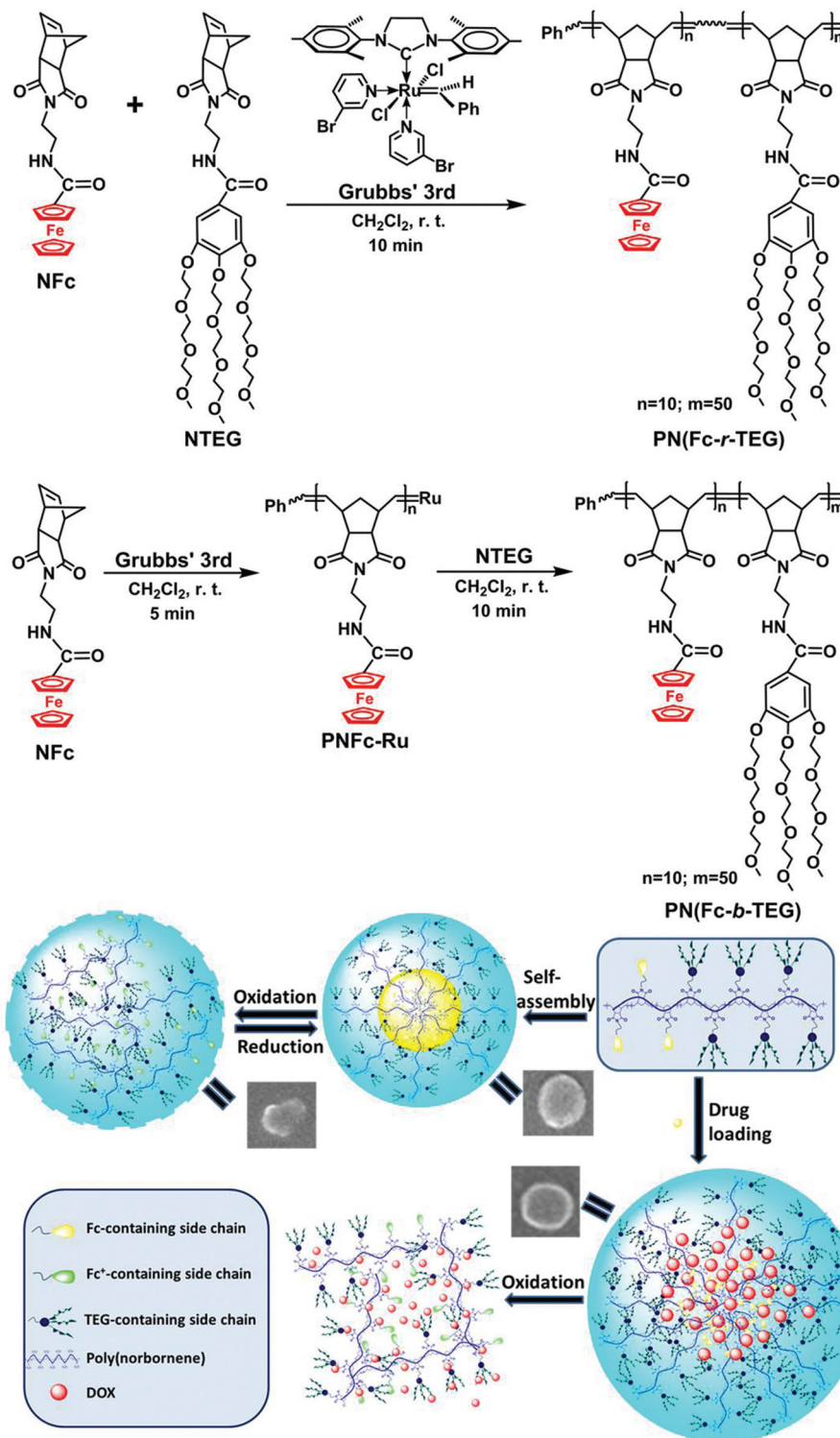
<sup>b</sup>National Engineering Laboratory for Clean Technology of Leather Manufacture, Sichuan University, Chengdu 610065, China

<sup>c</sup>College of Food and Bioengineering, Xihua University, Chengdu 610039, China. E-mail: wang\_weixiang@hotmail.com

†Electronic supplementary information (ESI) available. See DOI: 10.1039/c9py00332k

could be mediated by the type and concentration of oxidants.<sup>35</sup> Other researchers reported redox-responsive linear Fc-containing amphiphilic block copolymers that can self-assemble into different shapes including spherical micelles, hollow nano-

capsules (NCs), vesicles, nanotubes, nanoparticles (NPs) and multilayer films, for drug-loading and subsequent oxidation-controlled release of loaded molecules.<sup>36–41</sup> However, poly-norbornene-based Fc-containing amphiphilic copolymers have



**Scheme 1** Synthesis routes of PN(Fc-b-TEG) and PN(Fc-r-TEG), and graphical summary of the redox-controlled micelles of PN(Fc-b-TEG) as drug carriers.

rarely been applied for DCSs, which is probably attributed to insufficient knowledge about their biosafety. Furthermore, most reported DCSs lack corresponding biological experiments to evaluate their safety in the biosome. Often, small mammalian models such as rats, rabbits and dogs are used as mature methods to assess the possible toxicities and biodistribution of drug carriers in humans because of the close homology for the mammalian genomes.<sup>42</sup> However, these experiments are often expensive and time-consuming to establish mammalian models, and thus cannot keep pace with the rapid development of DCSs. To solve this problem, one of the most promising *in vivo* model systems, namely zebrafish (*Danio rerio*), is attracting considerable attention for toxicity studies, owing to unparalleled advantages such as high cost-effectiveness, high fecundity, *etc.*<sup>42–47</sup>

Accordingly, we report here a powerful way to fabricate redox-responsive Fc-containing polynorbornene-based amphiphilic copolymers (Scheme 1) by “living” and “controlled” ring-opening metathesis polymerization (ROMP) that is an outstanding method to synthesize well-defined polymers.<sup>30,48</sup> The hydrophobic Fc units are grafted onto a polynorbornene framework and the dendronized triethylene glycol (TEG) units are also attached to afford copolymers with suitable water-solubility. The Fc- and TEG-containing block copolymer **PN(Fc-*b*-TEG)** was synthesized by using a one-pot two-step sequential ROMP route, while the random copolymer **PN(Fc-*r*-TEG)** was prepared for comparison by feeding the Fc- and TEG-containing monomer at the same time. The reversible redox-controlled self-assembly behaviors of the two copolymers were investigated in CH<sub>2</sub>Cl<sub>2</sub> by using FeCl<sub>3</sub> as oxidant and glutathione (GSH) as reductant. The self-assembled micelles are further tested to encapsulate a hydrophobic model dye molecule Nile red (NR) and an anticancer drug DOX, respectively, and the oxidation-triggered release behavior was investigated by using FeCl<sub>3</sub> as a stimulus. We also compared the difference between **PN(Fc-*b*-TEG)** and **PN(Fc-*r*-TEG)** in self-assembly behavior, reversible redox-stimuli response, drug loading and release. More importantly, the biotoxicity of the micelles formed by these new copolymers were carefully evaluated by murine fibroblast cells (L-929 cell) and model organism zebrafish embryos, and the results confirmed the excellent biological safety of these polynorbornene-based copolymers.

## 2. Experimental

### 2.1. General data

General data, including materials and instruments, are listed in the ESI.†

### 2.2. ROMP synthesis of **PN(Fc-*b*-TEG)**

Monomers **NFc** (20.0 mg, 0.048 mmol, 10 equiv.) and **NTEG** (190.6 mg, 0.2392 mmol, 50 equiv.) were dissolved in 0.4 and 1.8 ml of CH<sub>2</sub>Cl<sub>2</sub>, separately. Grubbs third-generation catalyst (4.2 mg, 0.00478 mmol, 1 equiv.) was placed into a small

Schlenk flask, dissolved in 0.3 ml of dry CH<sub>2</sub>Cl<sub>2</sub> and flushed with N<sub>2</sub> atmosphere. First, monomer **NFc** was transferred into the catalyst-containing flask and stirred for 5 min at room temperature (r.t.) under an N<sub>2</sub> atmosphere. After that, a CH<sub>2</sub>Cl<sub>2</sub> solution of monomer **NTEG** was added, and the obtained reaction mixture was further agitated vigorously until the peak at 6.22 ppm disappeared by checking *in situ* the <sup>1</sup>H NMR spectrum of the reaction mixture. Then, the catalyst was quenched by adding 0.5 ml of ethyl vinyl ether (EVE). The product was purified by precipitation from CH<sub>2</sub>Cl<sub>2</sub> with diethyl ether (Et<sub>2</sub>O) three times, and dried *in vacuo* until constant weight to obtain the diblock copolymer **PN(Fc-*b*-TEG)** as a yellowish-brown solid. Yield: 94%. <sup>1</sup>H NMR (400 MHz, CDCl<sub>3</sub>, 25 °C, TMS) δ<sub>ppm</sub>: 7.74 and 7.58 (br, NHCO of Fc and TEG blocks), 7.08–7.05 (br, ph), 5.59 and 5.47 (br, CH=), 4.72–4.65 (br, substituted (sub.) Cp, Cp = η<sup>5</sup>-C<sub>5</sub>H<sub>5</sub>), 4.32 (s, sub. Cp), 4.18–4.09 (m, free Cp and ph-OCH<sub>2</sub>CH<sub>2</sub>O), 3.76–3.50 (m, NCH<sub>2</sub>CH<sub>2</sub>N of TEG block, ph-OCH<sub>2</sub>CH<sub>2</sub>O and OCH<sub>2</sub>CH<sub>2</sub>O), 3.33 and 3.31 (s, 3 × OCH<sub>3</sub>), 3.20 (br, NCH<sub>2</sub>CH<sub>2</sub>N of Fc block), 2.97 (s, =CH-CH of polynorbornene), 2.66 and 2.42 (double broad, CH-CO of polynorbornene), 2.03 (br, =CHCHCH<sub>2</sub>), 1.51 (br, CH=CHCHCH<sub>2</sub>). <sup>13</sup>C NMR (100 MHz, CDCl<sub>3</sub>, 25 °C, TMS), δ<sub>ppm</sub>: 178.5 (CON), 167.2 (NHCO), 152.3 (ph), 141.0 (ph), 133.3, 132.1 (=CCH), 129.2 (ph), 106.7 (ph), 72.4, 71.3, 70.7, 70.6, 70.4, 69.9, 69.8, 69.7, 69.6, 68.9, 68.8, 68.5, 68.4, 68.2, 67.3, 67.2 (Cp and OCH<sub>2</sub>), 59.0 (OCH<sub>3</sub>), 52.2 (ph-O-CH<sub>2</sub>), 50.8 (=CHCHCH), 45.7 (CH<sub>2</sub> of cyclopentane), 42.6 (=CH-CH), 41.2 (NCH<sub>2</sub>CH<sub>2</sub>N), 38.4 (NCH<sub>2</sub>CH<sub>2</sub>N). Selected IR (KBr, cm<sup>-1</sup>): 3443 (ν<sub>NH</sub>), 2922 (ν<sub>CH<sub>2</sub></sub>), 1768 (δ<sub>C=C</sub>), 1697 (δ<sub>NC=O</sub>), 1640 (δ<sub>NHC=O</sub>), 1111 (ν<sub>C-O-C</sub>), 852 (ν<sub>FeH</sub>).

### 2.3. General self-assembly procedure in water

5 mg of **PN(Fc-*b*-TEG)** was dissolved at r.t. in 5 ml of THF, followed by the dropwise addition of 5 ml of deionized water with vigorous stirring. After 2 h of stirring, the mixture was dialyzed against deionized water for 72 h by using a dialysis bag with a molecular weight cutoff (MWCO) of 3500 g mol<sup>-1</sup>, and during this period, the fresh dialysate was replaced every 4 h to remove THF completely. After dialysis, the micelle solution was obtained at a concentration of 0.5 mg ml<sup>-1</sup>. For **PN(Fc-*r*-TEG)**, a similar self-assembly procedure was used to prepare the corresponding micelle solution.

### 2.4. Oxidation–reduction response of micelles

200 mg of **PN(Fc-*b*-TEG)** was dissolved in 5 ml of dry CH<sub>2</sub>Cl<sub>2</sub> in a small Schlenk flask. Then a small amount of FeCl<sub>3</sub> dissolved in dry acetonitrile (0.5 ml) was added into the solution at r.t. with vigorous stirring for 10 min. After that, the UV-vis absorbance at 420 nm (the absorption band of the Fc group in the reduced state) totally disappeared and the solution changed from yellow to blue–green. To reduce the oxidized **PN(Fc-*b*-TEG)** solution, a certain amount of GSH was added into the above solution and stirred for several minutes until the yellow color was completely recovered to yield **PN(Fc-*b*-TEG)**. A similar procedure was adopted for the oxidation and reduction of **PN(Fc-*r*-TEG)**.

## 2.5. Loading and release of NR

**PN(Fc-*b*-TEG)** (5 mg) and NR (0.5 mg) were added into a 10 ml volumetric flask and dissolved in 5 ml of THF. After the polymer and NR were completely dissolved, dialysis (MWCO = 3500 g mol<sup>-1</sup>) was then carried out against deionized water to remove the solvent until no UV-vis absorption peak was observed at 580 nm (the characteristic absorption band of NR) in the dialysate. The stable NR-loaded micelle solution was obtained after removing the sedimentary NR in a dialysis bag. A similar drug-loading procedure was adopted for **PN(Fc-*r*-TEG)**. In the NR release experiment, a small amount of FeCl<sub>3</sub> solution was added directly into the solution of micelles in water, and the UV-vis absorption was monitored at different intervals to indicate the release of NR.

## 2.6. Loading and releasing of DOX

**PN(Fc-*b*-TEG)** (5 mg) and anticancer drug DOX (1 mg) were added into a 10 ml volumetric flask and dissolved in 5 ml of THF. After DOX and polymer were completely dissolved, 5 ml of deionized water was dropwise added into the flask. The obtained mixture solution was further stirred at r.t. for 2 h to obtain the DOX-loaded micelles that were then dialyzed (MWCO = 7000 g mol<sup>-1</sup>) against deionized water. The removal of unloaded DOX was monitored by determining the UV-vis absorption of the dialysate at 485 nm, and the dialysis treatment was stopped when there was no absorption in the dialysate. The drug loading content (DLC) and the encapsulation efficiency (EE) were determined according to the following formulae:

$$\text{DLC \%} = \frac{W_{\text{loaded drug}}}{W_{\text{micelles+loaded drugs}}} \times 100\%$$

$$\text{EE \%} = \frac{W_{\text{loaded drug}}}{W_{\text{free drug}}} \times 100\%$$

A similar DOX-loading procedure was adopted for the case of **PN(Fc-*r*-TEG)**. In the drug release experiment, 10 ml of the DOX-loaded micelles, obtained as described above, was added into a dialysis tube (MWCO = 3500 g mol<sup>-1</sup>), and then immersed at r.t. in 10 ml of different concentration FeCl<sub>3</sub> solutions.

## 2.7. Evaluation of the biotoxicity by L-929 cell

Murine fibroblast cells (L-929 cell), purchased from Cell Resource Center, Shanghai Institute of Life Sciences, Chinese Academy of Sciences, were cultured in Dulbecco's Modified Eagle's Medium (DMEM) containing 10% fetal bovine serum (FBS), 100 U ml<sup>-1</sup> penicillin and 100 mg ml<sup>-1</sup> streptomycin at 37 °C in a humidified atmosphere of 5% CO<sub>2</sub>. Copolymer-containing solutions with different concentrations, ranging from 8 to 0.0625 mg ml<sup>-1</sup>, were prepared by dissolving a certain amount of copolymer in deionized water. The sterilization of these solutions was carried out at 120 °C before toxicity testing. Cells were seeded in 96-well plates at 1 × 10<sup>4</sup> cells per ml and incubated for 24 h to allow attachment, and then 10 μl of the prepared copolymer-containing solution was added into

the plates and incubated for 1, 2 and 3 days (each sample contains three sets of parallel samples), respectively. 10 μl of CCK8 was added to each plate and incubated at 37 °C for 1.5 h. The absorbance was measured by a microplate reader (BIO-RAD550) at 570 nm. DMEM complete media with and without cells were used as positive and negative controls, respectively. The cell relative proliferation rate (RPR) was calculated by the following formula.

$$\text{RPR(\%)} = \frac{(\text{OD}_t - \text{OD}_n)}{\text{OD}_p - \text{OD}_n} \times 100\%$$

Here, OD<sub>t</sub>, OD<sub>p</sub> and OD<sub>n</sub> represent the absorbance values of test group, positive control group and negative control group, respectively. The relationship between the RPR and cytotoxicity grade is referred to the American Pharmacopoeia. As shown in Table S10,† grades 0 or 1 suggest good viability; grade 2 should be checked with cell morphological evaluation; while grades 3, 4 and 5 are unsatisfactory.

## 2.8. Evaluation of the acute embryo toxicity in zebrafish

The embryonic/larvae acute toxicity tests were conducted according to the literature report.<sup>49</sup> All animal procedures were performed in accordance with the Guidelines for Care and Use of Laboratory Animals of Xihua University and experiments were approved by the Animal Ethics Committee of Xihua University. 8 mg ml<sup>-1</sup> of micelles, obtained by the described method above, were utilized directly to confect the embryo culture medium (NaCl 3.5 g, KCl 0.05 g, NaHCO<sub>3</sub> 0.025 g and CaCl<sub>2</sub> 0.1 g per liter) for embryo exposure. In more detail, fertilized eggs were collected from AB strain zebrafish within 0.5–1 h post fertilization (hpf) and placed in fresh embryo culture medium without the copolymer. The healthy embryos were selected under the microscope (SZX10, Olympus, Japan) and distributed in 6-well microplates for exposure to the copolymer at 6 hpf. Three replicate experiments were conducted using various concentrations (8, 4 and 0.5 mg ml<sup>-1</sup>) of micelles of **PN(Fc-*b*-TEG)** and **PN(Fc-*r*-TEG)**, respectively, to observe the effects on mortality, malformation rate and hatching rate, to assess the toxicity of the copolymers. After 96 hpf, the hatched larvae were dyed by acridine orange (AO) to check the level of cell death. The zebrafish larvae after 96 hpf were stained in 2 mg l<sup>-1</sup> of AO staining solution at 28.5 °C for 30 min in the dark. After incubation, the embryos were rinsed with embryo media three times and anesthetized with 0.08% of 2-phenoxyethanol for 5 min. Next, the dyed larvae were observed under a fluorescence microscope. Green fluorescence was strengthened in the apoptosis region and weakened at the inhibitory site.

# 3. Results and discussion

## 3.1. ROMP synthesis of **PN(Fc-*b*-TEG)** and **PN(Fc-*r*-TEG)**

The amphiphilic **PN(Fc-*b*-TEG)** side-chain containing the Fc group and dendronized TEG branches was synthesized by chain extension of the Fc-containing homopolymer **PNFc** (with

ruthenium (Ru) end, which was reported by our group and shown in detail in the ESI,<sup>†</sup> to the second dendronized hydrophilic monomer NTEG, the synthesis of which has been described in our previous work,<sup>25</sup> via one-pot two-step sequential ROMP using the Grubbs third-generation catalyst at r.t. in dry CH<sub>2</sub>Cl<sub>2</sub>. The feed molar ratio of [monomer NFc]:[monomer NTEG]:[Grubbs 3<sup>rd</sup>] is 10:50:1, and the synthetic route is shown in Scheme 1. Specifically, the Fc-containing homopolymer PN<sub>2</sub>Fc-Ru was first obtained by the ROMP reaction of monomer NFc in dry CH<sub>2</sub>Cl<sub>2</sub> and then used as a macromolecular initiator to trigger the ROMP of monomer NTEG in dry CH<sub>2</sub>Cl<sub>2</sub> to produce PN(Fc-*b*-TEG). Furthermore, the PN(Fc-*r*-TEG) was acquired by mixing the monomers NFc and NTEG uniformly at the above mentioned molar ratio and adding them into the catalyst synchronously, and its detailed synthesis is shown in the ESI.<sup>†</sup>

It took 5 min to accomplish the ROMP of monomer NFc with 100% conversion according to the previous study,<sup>26</sup> and then monomer NTEG in dry CH<sub>2</sub>Cl<sub>2</sub> was added, and a kinetic study was conducted to monitor the polymerization of NTEG in CH<sub>2</sub>Cl<sub>2</sub> through *in situ* <sup>1</sup>H NMR analysis. A small amount of mixture reaction solution was taken out and inactivated by EVE at different time intervals and dried to measure the <sup>1</sup>H NMR spectrum in CDCl<sub>3</sub>. The monomer NTEG was totally converted when the peak of the olefinic protons at 6.22 ppm disappeared. As shown in Fig. S48,<sup>†</sup> only 10 min is needed for the second block to achieve 100% conversion. The rapid reaction rate indicates that ROMP is an effective strategy to synthesize the well-defined PN(Fc-*b*-TEG). For the fabrication of PN(Fc-*r*-TEG), a similar kinetic study was also conducted and the results showed that it also took only 10 min to realize the complete conversion of both monomers NFc and NTEG (Fig. S57<sup>†</sup>).

The successful combination of the second TEG block into the first Fc block is well confirmed by the appearance of several characteristic signals corresponding to the Fc and TEG structures. Fig. 1 shows the <sup>1</sup>H NMR spectrum of PN(Fc-*b*-TEG) in CDCl<sub>3</sub>. The peak at 7.74 ppm is attributed to the acylamino group of the TEG-containing block, and its phenyl protons are observed at 7.08–7.05 ppm. The characteristic protons of terminal OCH<sub>3</sub> groups are situated at 3.34–3.31 ppm, and the OCH<sub>2</sub> protons in the TEG units are observed at 3.76–3.50 ppm. For the Fc-containing block, the peak at 7.58 ppm is assigned to the acylamino group and the double peak signal at 4.72 and 4.65 ppm arises from the substituted cyclopentadienyl (Cp) protons close to the carbonyl group, while the other substituted Cp protons are located at 4.32 ppm. The broad peak at 3.20 ppm is attributed to methylene protons in the side chain of the first Fc block. All the above results adequately prove the integrity of the Fc-containing block and the successful introduction of the second TEG block by ROMP. In the <sup>13</sup>C NMR spectrum of PN(Fc-*b*-TEG) in CDCl<sub>3</sub> (Fig. S42<sup>†</sup>), the carbons of the carbonyl and acylamino groups are observed at 178.5 and 167.2 ppm, and the carbons of the benzene ring in the second TEG block are located at 152.3, 141, 129.2 and 106.7 ppm, respectively. The peaks at 133.3 and 132.1 ppm originate from the characteristic olefinic carbons of polynorbornene. The large number of peaks from 72.3 to 68.7 ppm are attributed to the carbons of OCH<sub>2</sub> groups in the TEG tails and the carbons of Fc group, while the carbons of OCH<sub>3</sub> are located at 58.9 ppm. All the other peaks of the <sup>1</sup>H and <sup>13</sup>C NMR spectra are clearly assigned and match well with the structure of PN(Fc-*b*-TEG). The UV-vis spectrum in CH<sub>2</sub>Cl<sub>2</sub> of PN(Fc-*b*-TEG) (Fig. S43<sup>†</sup>) shows a characteristic absorption band with a maximum peak (λ<sub>max</sub>), as expected, at 439 nm that is consistent with the integrity of the Fc group. To summarize, these

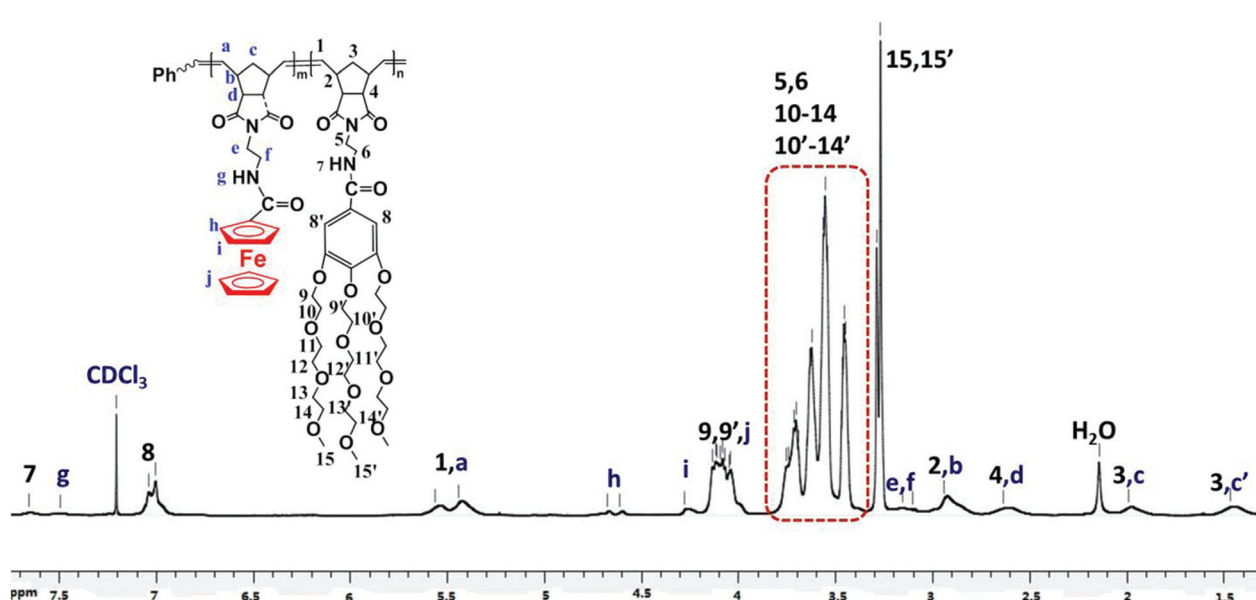


Fig. 1 <sup>1</sup>H NMR spectrum of PN(Fc-*b*-TEG) in CDCl<sub>3</sub>.

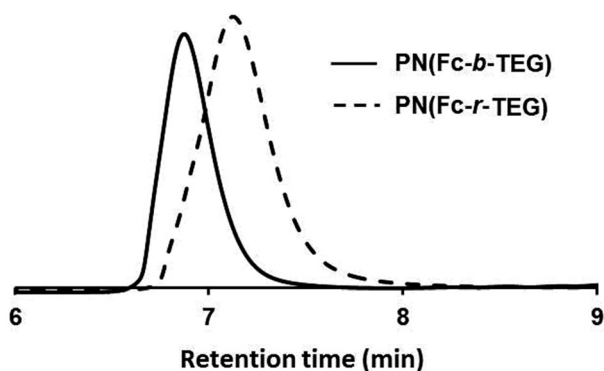


Fig. 2 GPC curves of PN(Fc-*b*-TEG) and PN(Fc-*r*-TEG).

data above mentioned provide strong proof for the formation of the second TEG block, and the integrity of the first Fe-containing block.

The polymerization degree of the first (Fc-containing) block, was first calculated by end-group analysis (see detailed description in the ESI†) using the  $^1\text{H}$  NMR spectrum of **PNFc** in  $(\text{CD}_3)_2\text{SO}$ , and the obtained value of  $10 \pm 1$  was then adopted to estimate the polymerization degree of the second TEG block by comparing the signal intensity of the substituted Cp with that of characteristic protons in the second TEG block using the  $^1\text{H}$  NMR spectrum of **PN(Fc-*b*-TEG)** in  $(\text{CD}_3)_2\text{SO}$  (Fig. S47†). Namely, the integration of the substituted Cp protons at 4.67 ppm was compared with those of the acylamino proton for the second block at 8.46 ppm, side-chain phenyl protons at 7.09 ppm, and the methylic protons at 3.20 ppm, respectively. The calculated polymerization degree of the second TEG block is  $50 \pm 5$ , showing an excellent agreement with the theoretical value of 50 from the  $^1\text{H}$  NMR conversions. GPC was also adopted to detect the molecular weight (MW) of **PN(Fc-*b*-TEG)** and the result shows an  $M_n$  value of 24 900 Da with polydispersity index (PDI) of 1.15 by using polystyrene (PS) as the standard (Table S6†). Owing to the large structural difference between the PS standard and the block copolymer, the MW obtained is smaller than the theoretical value calculated by the molar feed ratio and the corresponding monomer conversion.<sup>50</sup> More importantly, the small PDI value of 1.15 obtained from the GPC trace (Fig. 2), further demonstrated the controlled polymerization of the two blocks in **PN(Fc-*b*-TEG)** by ROMP. Furthermore, the random copolymer **PN(Fc-*r*-3TEG)** was also synthesized and well characterized by many techniques, and the corresponding results are provided in the ESI† for comparison in the following applications.

### 3.2. Micelles of PN(Fc-*b*-TEG) and PN(Fc-*r*-TEG) in water

Block copolymers with both hydrophilic and hydrophobic segments often show an amphiphilic character, and thus can self-assemble into a variety of interesting nanostructures with determined molecular arrangement and diverse morphologies such as spheres, vesicles, rodlike, and so on, in selective solutions.<sup>51,52</sup> In the current work, the yellow solid product **PN**

Table 1 Analysis results of pure micelles and drug-loaded micelles

	DA <sub>SEM</sub> <sup>a</sup> / nm	HDR <sub>DLS</sub> <sup>a</sup> / nm	CMC/ mg ml <sup>-1</sup>	DLC (%)	EE (%)
<b>PN(Fc-<i>b</i>-TEG)</b>					
Original	101 ± 10	156	0.11		
Oxidized	113 ± 40	190	0.246		
Reduced	93 ± 20	138			
<b>PN(Fc-<i>r</i>-TEG)</b>					
Original	81 ± 25	159	0.17		
Oxidized		250	0.305		
Reduced		164			
<b>PN(Fc-<i>b</i>-TEG)-NR</b>					
<b>PN(Fc-<i>r</i>-TEG)-NR</b>					
<b>PN(Fc-<i>b</i>-TEG)-DOX</b>	129 ± 10	193		7.4	66.7
<b>PN(Fc-<i>r</i>-TEG)-DOX</b>	89 ± 20	226		3.3	21.1

<sup>a</sup> DA<sub>SEM</sub> is the average diameter from SEM analysis; HDR<sub>DLS</sub> is the hydrodynamic radius from DLS.

(**Fc-*b*-TEG**), obtained by precipitation from  $\text{CH}_2\text{Cl}_2$  with  $\text{Et}_2\text{O}$ , contains a hydrophobic Fc-containing block and hydrophilic TEG segment, and thus is expected to self-assemble into interesting nanostructures in aqueous solution. The critical micelle concentration (CMC) of **PN(Fc-*b*-TEG)** was detected by the pyrene fluorescence technique.<sup>53</sup> Additionally, this method was also applied for the CMC determination of **PN(Fc-*r*-TEG)**. Fig. S59† shows the results of fluorescence emission spectra with different concentrations and the corresponding plot of the  $I_3/I_1$  ratios vs. logarithmic concentration. The determined value of the CMC is  $0.11 \text{ mg ml}^{-1}$  for **PN(Fc-*b*-TEG)**, cf.  $0.17 \text{ mg ml}^{-1}$  for **PN(Fc-*r*-TEG)** (Table 1). The higher CMC value of **PN(Fc-*r*-TEG)** is due to its better water-solubility than **PN(Fc-*b*-TEG)**. The random distribution of hydrophilic and hydrophobic components in the random copolymer is advantageous for its dissolution in water. The self-assembly process of **PN(Fc-*b*-TEG)** was triggered by dissolving the copolymer in a certain amount of THF and then adding water dropwise, and the organic solvent was then removed by dialysis treatment against distilled water. As shown in Fig. S58,† the Tyndall effect was clearly observed when a beam of light was applied across the mixture solution, indicating the formation of aggregates through the self-assembly of the amphiphilic copolymers. The self-assembled micelles, acquired by the above method with a concentration  $0.5 \text{ mg ml}^{-1}$ , were further investigated in detail by dynamic laser scattering (DLS) measurements and scanning electron microscopy (SEM). As shown in Fig. 3A and Table 1, nearly spherical micelles were observed with size of  $101 \pm 10 \text{ nm}$  by SEM. These micelles exhibit bright peripheries and dark cores. A similar phenomenon was also observed for the micelles of **PN(Fc-*r*-TEG)** with average size of  $81 \pm 25 \text{ nm}$  (Fig. S54†). However, it is worth mentioning that the shape and size of these micelles are more inhomogeneous, which is probably caused by the randomness of **PN(Fc-*r*-TEG)**. Moreover, DLS (Fig. 4A, S53† and Table 1) provides a hydrodynamic diameter (HDR<sub>DLS</sub>) of 156 nm with a PDI of 0.246 for the micelles of **PN(Fc-*b*-TEG)** and 159 nm with PDI of 0.288 for

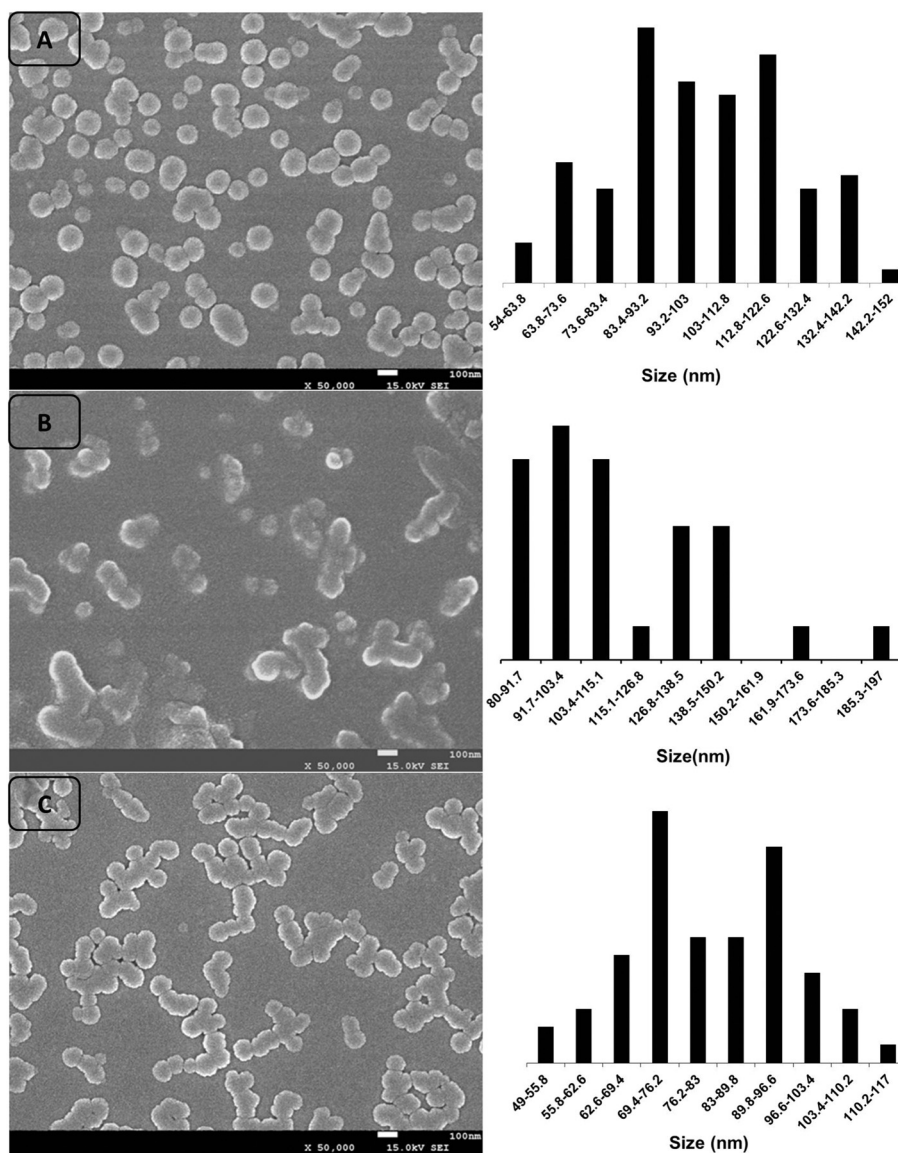


Fig. 3 SEM images of micelles self-assembled by PN(Fc-*b*-TEG) (A) in aqueous solution and of PN(Fc-*b*-TEG) oxidized with FeCl<sub>3</sub> (B) and then reduced with GSH (C).

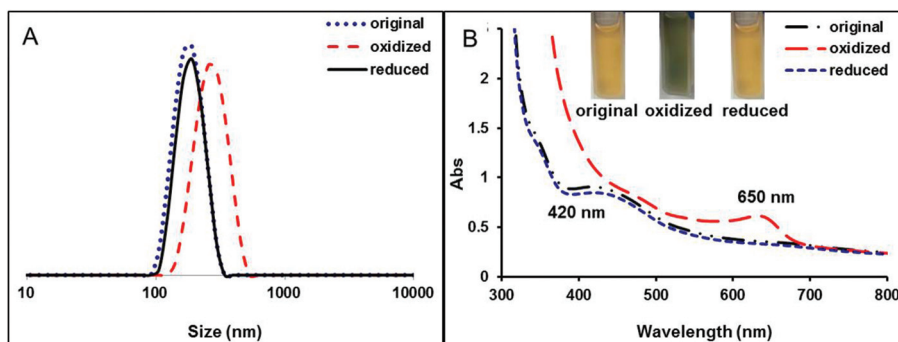


Fig. 4 (A) DLS curves of micelles of PN(Fc-*b*-TEG) in water during an oxidation–reduction cycle. (B) UV–Vis spectra and photographs of PN(Fc-*b*-TEG) in CH<sub>2</sub>Cl<sub>2</sub> during an oxidation–reduction cycle.

those of **PN(Fc-*r*-TEG)**, respectively. The size obtained by SEM is typically smaller than the value determined by using DLS, which arises from their different determination conditions. More specifically, DLS determines the size of micelles in the hydrodynamic state with swollen cores and stretched shells, while the size tested by SEM indicates the conformation of micelles in the dry state.<sup>54,55</sup>

### 3.3 Reversible redox self-assembly of **PN(Fc-*b*-TEG)** and **PN(Fc-*r*-TEG)**

In the field of stimuli-responsive polymer systems, the Fc group is widely used as a hydrophobic block to construct amphiphilic block copolymers to achieve a redox-response because of its reversible redox activity.<sup>18</sup> The reversible redox-response behavior of the two Fc-containing copolymers **PN(Fc-*b*-TEG)** and **PN(Fc-*r*-TEG)** was investigated through UV-vis spectroscopy by using FeCl<sub>3</sub> as oxidant and GSH as reductant. As shown in Fig. 4B, a broad absorption peak at 420 nm is clearly observed for the original **PN(Fc-*b*-TEG)** in CH<sub>2</sub>Cl<sub>2</sub>, and this peak is the characteristic absorbance band of the Fc group in the reduced state. The characteristic UV-vis absorption peak at 420 nm gradually disappeared with the increase of the amount of oxidant, and a new absorption peak was observed at 650 nm owing to the oxidation of the Fc group into ferrocenium (Fcium). A more clear and intuitive fact is that the color of the solution changed from yellow to green due to the oxidation of the Fc group. Interestingly, after the reducing agent of GSH was added into the oxidized solution, the characteristic signal at 420 nm re-emerged and the color of the solution returned back to yellow, which is attributed to the reduction of oxidized Fcium moieties into Fc in the reduced state.<sup>56</sup> This information provides a convincing proof for the reversible redox of this Fc-containing amphiphilic copolymer.

The redox-responsive self-assembly of the amphiphilic block copolymer **PN(Fc-*b*-TEG)** was further investigated by SEM, DLS and the pyrene fluorescence technique. As mentioned above, the **PN(Fc-*b*-TEG)** can self-assemble into spherical micelles in aqueous solution. After being oxidized by FeCl<sub>3</sub>, the morphology and size distribution are more irregular compared with the original state. The micelles were broken to form larger aggregates, and the size of the micelles changed to 113 ± 40 nm according to SEM (Fig. 3B). The size and shape variation are primarily due to the fact that hydrophobic Fc groups are converted to the hydrophilic Fcium structures, and this change results in an increase of the hydrophilicity of the micelles and electrostatic repulsion among the positively charged Fcium species.<sup>39,40,56</sup> The CMC values of the micelles after oxidation by FeCl<sub>3</sub> was also studied by using the pyrene fluorescence probe method, and Fig. S61† provides values of 0.246 and 0.305 mg ml<sup>-1</sup> for the oxidized **PN(Fc-*b*-TEG)** and **PN(Fc-*r*-TEG)**, respectively. This increase in CMC values is also caused by the higher solubility arising from the oxidized Fcium groups. Furthermore, it is worth noting that the oxidized micelles can be reversibly restored to the reduced form by adding GSH reducing agent. As shown in Fig. 3C, the SEM image presents a uniform particle size of 93 ± 20 nm, which is

matched well with the original size and shape. Meanwhile, the results of DLS (Fig. 4A and S60†) show that the oxidized micelles have an average diameter of 190 nm for **PN(Fc-*b*-TEG)** and 250 nm for **PN(Fc-*r*-TEG)**, while the reduced micelles have average diameters of 138 and 164 nm for **PN(Fc-*b*-TEG)** and **PN(Fc-*r*-TEG)**, respectively. Both of these results for the reduced state are close to the original ones, which further demonstrates that the redox-controlled reversible self-assembly of amphiphilic copolymer **PN(Fc-*b*-TEG)** and **PN(Fc-*r*-TEG)** can be successfully accomplished in aqueous solution by redox stimuli. Overall, the redox-responsive behavior of these copolymer micelles indicates their potential possibilities as controllable DCSs.

### 3.4 Drug loading and release

**PN(Fc-*b*-TEG)** and **PN(Fc-*r*-TEG)** can self-assemble into spherical micelles, as mentioned above, with the redox-responsive Fc segments forming the core and TEG-containing part as the shell, which endows the possibility for the encapsulation and controlled release of small fluorescent molecules upon an external oxidation stimulus. The water insoluble model drug NR was chosen to be encapsulated into the hydrophobic interior of micelles in an aqueous environment. A clear red solution (Fig. S65a†) was obtained after dissolving the block copolymer **PN(Fc-*b*-TEG)** and NR in THF. The drug loading process was triggered by dialyzing against water to slowly exchange the organic non-polar solvent with the polar solvent (water) that is selective for the TEG block. As shown in Fig. S65b,† a change in color was observed, which is typical for NR when it is stabilized in an aqueous phase. The same operation was also carried out for **PN(Fc-*r*-TEG)**. The obtained NR-loaded micelles, denoted as **PN(Fc-*b*-TEG)-NR** and **PN(Fc-*r*-TEG)-NR**, respectively, were characterized by SEM, DLS and UV-vis spectroscopy. The UV-vis spectrum showed a broad λ<sub>max</sub> peak at 560 nm for both NR-loaded micelles, corresponding to the characteristic absorption band of NR in aqueous solution (Fig. S64†). Notably, the **PN(Fc-*b*-TEG)** exhibits a higher loading ability than **PN(Fc-*r*-TEG)** at the same conditions according to the UV-vis absorbance strength (Fig. S64 and S70†). SEM images showed spherical NR-loaded micelles for **PN(Fc-*b*-TEG)-NR** with average diameter of 130 ± 15 nm (Fig. S62†) for **PN(Fc-*r*-TEG)-NR** (Fig. S68†) of 93 ± 30 nm. Both of these results indicate a larger average size than for the original unloaded micelles, owing to the encapsulation of NR in the hydrophobic core. DLS curves indicated a hydrodynamic radius of 226 nm for **PN(Fc-*b*-TEG)-NR** (Fig. S63† and Table 1), and 308 nm for **PN(Fc-*r*-TEG)-NR** (Fig. S69† and Table 1), respectively. The larger size from DLS, compared with the original micelles, also further supported that the water-insoluble NR was encapsulated in the hydrophobic core of the micelles. The controlled release of the encapsulated model compound NR was triggered by adding an oxidant after the successful transfer of NR into the micelles. A small amount of FeCl<sub>3</sub> aqueous solution was added into the solution of NR-loaded micelles in water, resulting in the release of the dye (see Fig. S65c, S66, S67 and S71†).

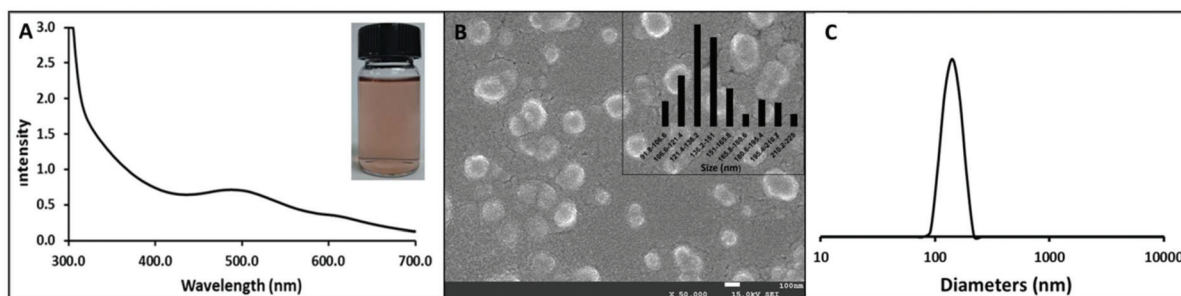


Fig. 5 The UV-vis absorption (A), SEM image (B) and DLS curve (C) of PN(Fc-*b*-TEG)-DOX micelles.

Furthermore, the anticancer drug DOX, which has been widely applied for cancer therapy, was employed to ascertain the drug-loading ability of the present micelles. First, a certain amount of copolymer and DOX were dissolved in THF and deionized water was then added slowly. The mixed solution was vigorously stirred for 2 h and then transferred into the dialysis bag with MWCO of 7000 g mol<sup>-1</sup>, and the dialysis treatment against deionized water was then carried out until the THF was completely removed and the dialysate showed no characteristic UV-vis absorbance of DOX at 480 nm. The finally obtained micelles were denoted as PN(Fc-*b*-TEG)-DOX and PN(Fc-*r*-TEG)-DOX, respectively, and were further investigated.

The successful encapsulation of DOX by the formed micelles was confirmed by comparing the UV-vis absorption spectra of the original and DOX-loaded micellar solutions. The latter shows a characteristic absorption peak of DOX at 480 nm as shown in Fig. 5A. The loaded content of DOX was determined by the standard curve of DOX in aqueous solution drawn by using its  $\lambda_{\max}$  at 480 nm (Fig. S73†). For PN(Fc-*b*-TEG)-DOX, the DLC value was calculated to be 7.4%, and the EE was determined to be 66.7%. Furthermore, the SEM image shows an average size of 129 ± 10 nm (Fig. 5B), and the hydrodynamic radius of micelles was also detected by DLS and the result shows an average size of 193 nm with a PDI value of 0.424 (see Fig. 5C). For PN(Fc-*r*-TEG)-DOX, its DLC was evaluated to be 3.3% and the EE was 21.1%, while the SEM photograph shows an average size of 89 ± 20 nm (Fig. S80†), and the DLS provides the hydrodynamic radius of 226 nm with PDI value of 0.712 (Fig. S79†). The obvious differences in the drug-loading ability and size distributions of the two types of micelles can be attributed to the molecular structure differences between PN(Fc-*b*-TEG) and PN(Fc-*r*-TEG). The differences between PN(Fc-*b*-TEG) and PN(Fc-*r*-TEG) are summarized in Table 1 from which it is clear that the micelles of PN(Fc-*b*-TEG) have better ability for drug-loading.

The release of encapsulated DOX was triggered by the addition of FeCl<sub>3</sub> as oxidant. In more detail, the DOX-loaded micellar solution was dialyzed against a solution of FeCl<sub>3</sub> with different concentrations. The release of DOX was confirmed by the increasing of UV-vis absorption at 480 nm of the solution outside the dialysis bag. A certain volume of deionized water solution was withdrawn from the beaker at certain time intervals to test the UV-vis absorption and the same volume of

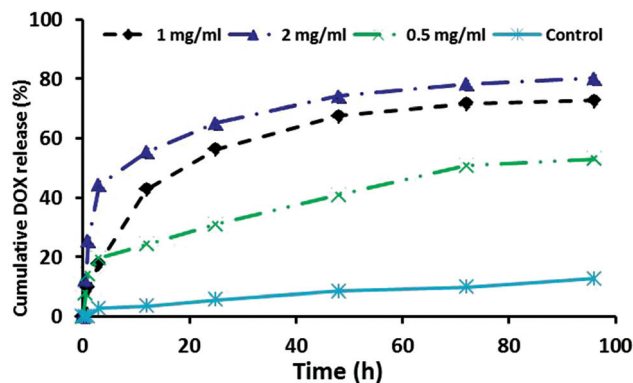


Fig. 6 The cumulative release of the PN(Fc-*b*-TEG)-DOX at different concentrations of FeCl<sub>3</sub>.

fresh buffer solution was added to keep the volume constant. The cumulative release of DOX at different oxidant concentrations was calculated by using its standard curve. As shown in Fig. S83,† the cumulative release rate of DOX for the micelles of PN(Fc-*r*-TEG)-DOX reached 45% within 12 h and 64% at 96 h, while the corresponding values for PN(Fc-*b*-TEG)-DOX were 42 and 73% (Fig. 6) using the same oxidant concentration (1 mg ml<sup>-1</sup>). The DOX loaded in the micelles of PN(Fc-*r*-TEG) shows a faster release rate at the pre-stage and lower cumulative release rate compared with the PN(Fc-*b*-TEG), which is due to the irregular molecular structure and lower drug loading capacity for the random copolymer. Besides, with the increasing of oxidant concentration, a significant increase in cumulative release was observed, indicating that the drug release process can be controlled by the amount of oxidant. We also found low release of DOX molecules from samples without the treatment of oxidants, which is perhaps because DOX can be adsorbed onto the surface of the vesicles or shows slow diffusion from the micelles. In short, these Fc-containing micelles can be used as DCSs, considering the important role of redox reactions, to load functional molecules which can be released in a controlled method upon oxidation stimuli.

### 3.5. Biototoxicity evaluation

**3.5.1. *In vitro* toxicity in L-929 cells.** An ideal drug carrier should exhibit good biocompatibility with no side effects on

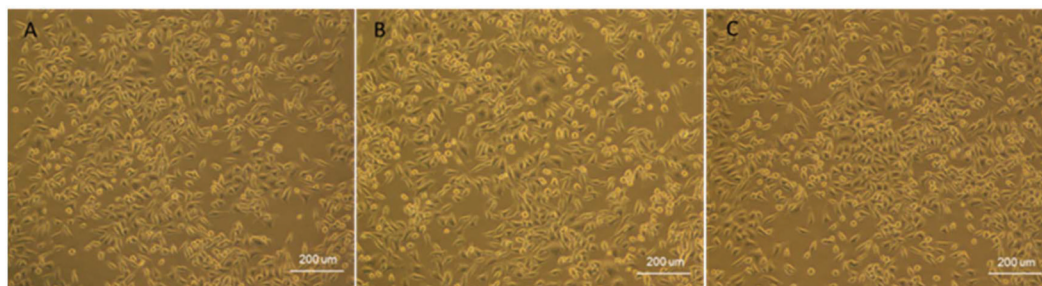


Fig. 7 Adherent covered L929 cells after three days of culture: (A) control group; (B) PN(Fc-*b*-TEG) treated group ( $8 \text{ mg ml}^{-1}$ ); (C) PN(Fc-*r*-TEG) treated group ( $8 \text{ mg ml}^{-1}$ ).

life-forms. Here, the toxicity of the present carriers formed by PN(Fc-*b*-TEG) and PN(Fc-*r*-TEG) was studied by CCK assay that has been widely applied in the field of drug screening, cell proliferation assay, cytotoxicity assay, tumor drug sensitivity test and biological factor activity tests in L-929 cells. A series of PN(Fc-*b*-TEG) and PN(Fc-*r*-TEG) concentrations ranging from 8 to  $0.0625 \text{ mg ml}^{-1}$  were adopted to measure their cell toxicity *in vitro*. The results showed that both copolymers had no obvious cell proliferation toxicity even at the maximum concentration of  $8 \text{ mg ml}^{-1}$  after mixed cultivation for 3 d (Fig. 7). According to the results of RPR (Fig. 8), the cyto-

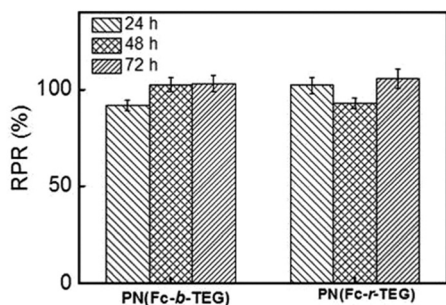


Fig. 8 The RPRs of L929 cells incubated with PN(Fc-*b*-TEG) and PN(Fc-*r*-TEG) ( $8 \text{ mg ml}^{-1}$ ).

toxicity classification is grade 0. Interestingly, partial results of the RPR surpassed 100% at a micelle concentration of  $8 \text{ mg ml}^{-1}$ , probably owing to the unique copolymer composition that is beneficial for cell growth and proliferation. The cell-related experiments results proved that both PN(Fc-*b*-TEG) and PN(Fc-*r*-TEG) had excellent biocompatibility with L929 cells.

**3.5.2. *In vivo* acute embryo toxicity in zebrafish.** To further understand the safety of these carriers formed by PN(Fc-*b*-TEG) and PN(Fc-*r*-TEG), zebrafish embryo, as a rapid, medium throughput, cost-effective whole animal model, was used to provide a more comprehensive and predictive developmental toxicity evaluation. The results clearly indicate that the incidence of micelle-treated survival and hatching rate are not affected (Fig. 9). Besides, zebrafish embryos are transparent throughout every developmental stage and allow direct observation of the development of all internal organs. Therefore any morphological malformations such as pericardial oedema, yolk sac oedema, bent trunk and tail deformation could be examined directly by a stereo microscope. Notably, in the present cases, such morphological malformations were not observed in either the control and micelle-treated groups throughout the entire test period, and the embryos presented well-developed head, notochord, caudal fin, eyes, tail, yolk sac and pigment features (Fig. 10).

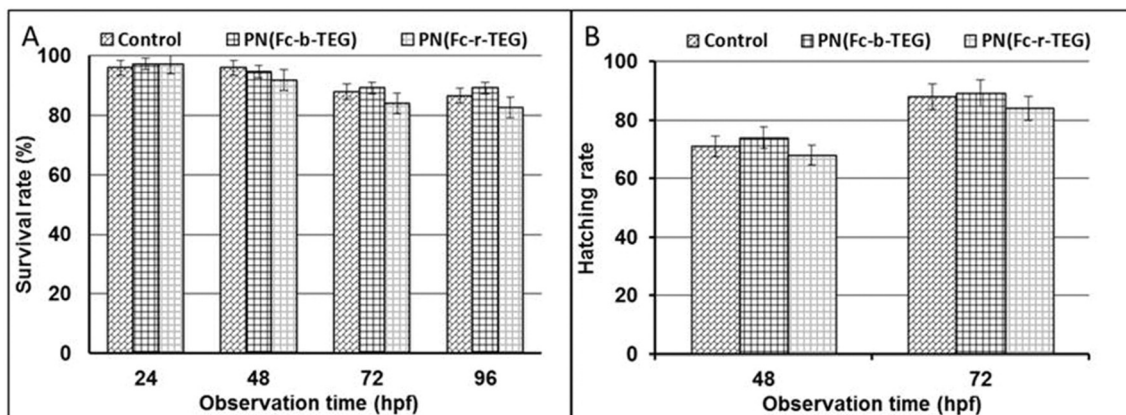
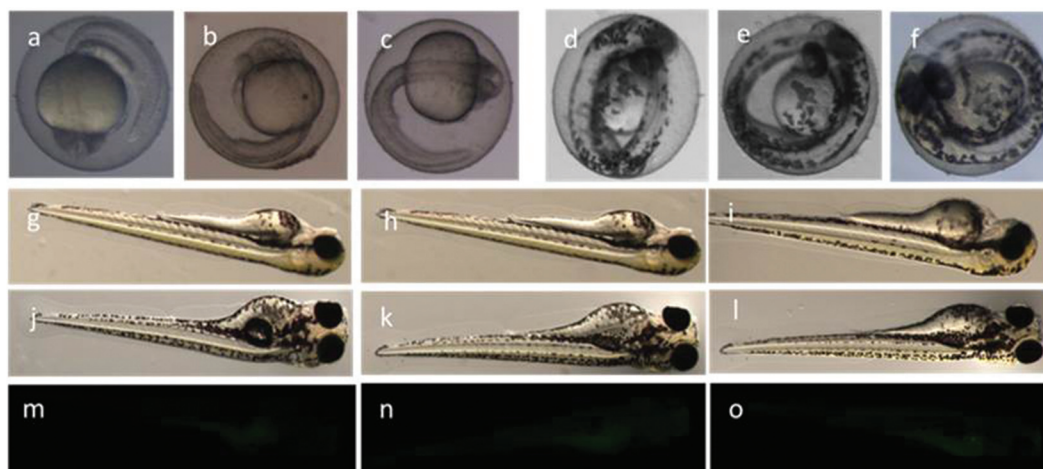


Fig. 9 Survival rates (A) and hatching rates (B) of zebrafish embryos at different time points in all treatments with micelles at concentration of  $8 \text{ mg ml}^{-1}$ .



**Fig. 10** Microscopic images of embryos, larvae and fluorescence: (a), (d), (g), (j) and (m) are controls; (b), (e), (h), (k) and (n) are samples treated with **PN(Fc-*b*-TEG)**; (c), (f), (i), (l) and (o) are samples treated with **PN(Fc-*r*-TEG)**. Images of (a)–(c) are the stage at 24 hpf; (d)–(f) are the stage at 48 hpf; (g)–(i) are the stage at 72 hpf; and (j)–(l) are the stage at 96 hpf. Images of (m)–(o) are obtained upon cellular apoptosis staining by AO at 96 hpf. All the experimental groups were treated with a concentration of  $8 \text{ mg ml}^{-1}$ .

**3.5.3 Cell death in live zebrafish.** AO, a nucleic acid-selective metachromatic dye, can permeate into apoptotic or necrotic cells to intercalate with partially uncoiled DNA and become highly fluorescent, whereas it is nonpermeable to normal cells, and so it is widely used for detecting sites of cell death in zebrafish.<sup>57</sup> To evaluate if *in vivo* exposure of copolymer micelles could induce cell death, zebrafish embryos were exposed to  $8 \text{ mg ml}^{-1}$  of copolymer micelles for 96 hpf and treated with AO for 0.5 h to stain dying cells. The presence of AO in the control larvae demonstrated that cell apoptosis was a normal physiological process during development (Fig. 10m). There was no difference in larvae exposed to copolymer micelles (Fig. 10n and o) in comparison to the control larvae, indicating that these drug carriers did not cause cellular apoptosis. Hence, this investigation strongly suggests that the Fc-containing micelles of **PN(Fc-*b*-TEG)** and **PN(Fc-*r*-TEG)** show no harm to cells and could be highly appropriate for biomedical and potential drug carrier applications.

## 4. Conclusions

In summary, we presented two new amphiphilic copolymers, block **PN(Fc-*b*-TEG)** and random **PN(Fc-*r*-TEG)**, which contain a polynorbornene backbone with side-chain hydrophobic Fc groups and hydrophilic dendronized TEG branches, by the controlled polymerization method of ROMP with the aid of a very efficient Grubbs third-generation ruthenium catalyst.<sup>34,58</sup> Nearly spherical micelles with size of  $101 \pm 10$  and  $81 \pm 25$  nm by SEM were formed as new potential drug carrier systems by the self-assembly of **PN(Fc-*b*-TEG)** and **PN(Fc-*r*-TEG)** in water, respectively. More importantly, the Fc group endowed reversible redox-response behavior for the amphiphilic copolymer, which could be utilized to trigger drug release. This hypothesis has been proved by drug loading and releasing experiments.

The hydrophobic dye NR was selected to be successfully encapsulated into the micelles and can be released under the redox stimuli. Furthermore, the anticancer drug DOX could also be loaded into the hydrophobic cores of the micelles, and the DLC reached 7.4 and 3% for the block and random copolymer, respectively. The release behavior of the DOX under addition of the gentle oxidant  $\text{FeCl}_3$  was studied and the results showed that the release ratio increased with increasing concentration of the oxidant. At the same conditions, the micelles of **PN(Fc-*r*-TEG)** carrying DOX showed faster release rate at the pre-stage and lower cumulative release rate compared with the micelles of **PN(Fc-*b*-TEG)**. Furthermore, the safety evaluation conducted by L929 cell and zebrafish embryo studies, revealed their excellent biological safety. Consequently, both of the exploited polynorbornene copolymers are promising polymer carriers that can form micelles to encapsulate drugs for the application of controlled drug delivery. However, comparing **PN(Fc-*r*-TEG)** with **PN(Fc-*b*-TEG)**, the latter displays much better qualities in terms of self-assembly, drug-loading and release properties, owing to its more regular molecular structure.

## Conflicts of interest

The authors declare no conflicts of interest in this article.

## Acknowledgements

This work was financially supported by the Science & Technology Department of Sichuan Province (No. 2018HH0038). The authors would like to thank Ms Wang Zhonghui (College of Light Industry, Textile and Food Engineering, Sichuan University) for her valuable help in DLS

measurements and Ceshigo (<http://www.ceshigo.com>) for help in SEM.

## References

- L. Xiong, Q. J. Luo, Y. Wang, X. D. Li, Z. Q. Shen and W. P. Zhu, *Chem. Commun.*, 2015, **51**, 14644–14647.
- P. Jha, *Nat. Rev. Cancer*, 2009, **9**, 655–664.
- T. Noyhouzer, C. L'Homme, L. Beaulieu, S. Mazurkiewicz, S. Kuss, H. B. Kraatz, S. Canesi and J. Mauzeroll, *Langmuir*, 2016, **32**, 4169–4178.
- D. Wirtz, K. Konstantopoulos and P. C. Searson, *Nat. Rev. Cancer*, 2011, **11**, 512–522.
- H. Yi, P. Liu, N. Sheng, P. Gong, Y. Ma and L. Cai, *Nanoscale*, 2016, **8**, 5985–5995.
- H. I. Yang, J. L. Zhao, C. Y. Wu, C. Q. Ye, D. W. Zou and S. G. Wang, *Chem. Eng. J.*, 2018, **351**, 548–558.
- L. Gandhi, D. Rodríguez-Abreu, E. Gadgeel, E. Esteban, E. Felip, F. De Angelis, M. Domine, P. Clingan, M. J. Hochmair and S. F. Powell, *N. Engl. J. Med.*, 2018, **378**, 2078–2092.
- H. Gelderblom, W. J. Loos, J. Verweij, M. E. L. van der Burg, M. J. A. de Jonge, E. Brouwer, K. Nooter, G. Stoter and A. Sparreboom, *Eur. J. Cancer*, 2002, **38**, 205–213.
- A. Gabizon, H. Shmeeda and Y. Barenholz, *Clin. Pharmacokinet.*, 2003, **42**, 419–436.
- D. Svirskis, J. Travas-Sejdic, A. Rodgers and S. Garg, *J. Controlled Release*, 2010, **146**(1), 6–15.
- M. R. Abidian, D. H. Kim and D. C. Martin, *Adv. Mater.*, 2006, **18**, 405–409.
- H. Abdelkader, A. W. Alani and R. G. Alany, *Drug Delivery*, 2014, **21**, 87–100.
- S. M. Lee and S. T. Nguyen, *Macromolecules*, 2013, **46**, 9169–9180.
- G. Liang, H. Ni, S. Bao, F. Zhu, H. Gao, Q. Wu and B. Z. Tang, *Langmuir*, 2014, **30**, 6294–6301.
- D. Jańczewski, J. Song, E. Csányi, L. Kiss, P. Blazsó, R. L. Katona, M. A. Deli, G. Gros, J. W. Xua and G. J. Vancso, *J. Mater. Chem.*, 2012, **22**, 6429–6435.
- Z. P. Xiao, Z. H. Cai, H. Liang and J. Lu, *J. Mater. Chem.*, 2010, **20**, 8375–8381.
- L. Peng, A. Feng, M. Huo and J. Yuan, *Chem. Commun.*, 2014, **50**, 13005–13014.
- H. B. Gu, S. D. Mu, G. R. Qiu, X. Liu, L. Zhang, Y. F. Yuan and D. Astruc, *Coord. Chem. Rev.*, 2018, **364**, 51–85.
- G. Saravanakumar, J. Kim and W. J. Kim, *Adv. Sci.*, 2017, **4**, 1600124.
- K. Kataoka, A. Harada and Y. Nagasaki, *Adv. Drug Delivery Rev.*, 2001, **47**, 113–131.
- L. Peng, S. Liu, A. Feng and J. Yuan, *Mol. Pharmaceutics*, 2017, **14**, 2475–2486.
- T. Liu, Z. Liu, J. Chen, R. Jin, Y. Bai, Y. Zhou and X. Chen, *J. Biomed. Nanotechnol.*, 2018, **14**, 1107–1116.
- Y. Liu, S. D. Mu, X. Liu, Q. J. Ling, Q. D. Hang, J. Ruiz, D. Astruc and H. B. Gu, *Tetrahedron*, 2018, **74**(37), 4777–4789.
- X. Liu, Q. J. Ling, L. Zhao, G. R. Qiu, Y. Wang, L. Song, Y. Zhang, J. Ruiz, D. Astruc and H. B. Gu, *Macromol. Rapid Commun.*, 2017, **38**, 1700448.
- X. Liu, G. R. Qiu, L. Zhang, F. F. Liu, S. D. Mu, Y. R. Long, Q. X. Zhao, Y. Liu and H. B. Gu, *Macromol. Chem. Phys.*, 2018, **219**, 1800273.
- L. Zhang, G. R. Qiu, F. F. Liu, X. Liu, S. D. Mu, Y. R. Long, Q. X. Zhao, Y. Liu and H. B. Gu, *React. Funct. Polym.*, 2018, **132**, 60–73.
- A. Rapakousiou, C. Deraedt, H. B. Gu, L. Salmon, C. Belin, J. Ruiz and D. Astruc, *J. Am. Chem. Soc.*, 2014, **136**, 13995–13998.
- H. B. Gu, R. Ciganda, R. Hernandez, P. Castel, P. X. Zhao, J. Ruiz and D. Astruc, *Macromolecules*, 2015, **48**, 6071–6076.
- H. B. Gu, R. Ciganda, R. Hernández, P. Castel, A. Vax, P. X. Zhao, J. Ruiz and D. Astruc, *Polym. Chem.*, 2016, **7**, 2358–2371.
- H. B. Gu, R. Ciganda, P. Castel, J. Ruiz and D. Astruc, *Macromol. Chem. Phys.*, 2018, **219**, 1800384.
- H. B. Gu, R. Ciganda, P. Castel, A. Vax, D. Gregurec, J. Irigoyen, S. Moya, L. Salmon, P. X. Zhao, J. Ruiz, R. Hernández and D. Astruc, *Chem.–Eur. J.*, 2015, **21**, 18177–18186.
- H. B. Gu, A. Rapakousiou, P. Castel, N. Guidolin, N. Pinaud, J. Ruiz and D. Astruc, *Organometallics*, 2014, **33**, 4323–4335.
- F. F. Liu, X. Liu, D. Astruc and H. B. Gu, *J. Colloid Interface Sci.*, 2019, **533**, 161–170.
- H. B. Gu, R. Ciganda, P. Castel, S. Moya, R. Hernandez, J. Ruiz and D. Astruc, *Angew. Chem., Int. Ed.*, 2018, **57**, 2204–2208.
- F. Xu, H. Li, Y. L. Luo and W. Tang, *ACS Appl. Mater. Interfaces*, 2017, **9**, 5181–5192.
- R. H. Staff, M. Gallei, K. Landfester and D. Crespy, *Macromolecules*, 2014, **47**, 4876–4883.
- S. J. Zhai, J. Shang, D. Yang, S. Wang, J. Hu and G. Lu, *J. Polym. Sci., Part A: Polym. Chem.*, 2012, **50**, 811–820.
- M. Saleem, L. Wang, H. J. Yu, Zain-ul-Abdin, M. Akram and R. S. Ullah, *Colloid Polym. Sci.*, 2017, **295**, 995–1006.
- L. Zhao, Q. J. Ling, X. Liu, C. D. Hang, Q. X. Zhao, F. F. Liu and H. B. Gu, *Appl. Organomet. Chem.*, 2018, **32**, e4000.
- L. C. Liu, L. L. Rui, Y. Gao and W. A. Zhang, *Polym. Chem.*, 2015, **6**, 1817–1829.
- C. Feng, G. Lu, Y. Li and X. Huang, *Langmuir*, 2013, **29**, 10922–10931.
- V. E. Fako and D. Y. Furgeson, *Adv. Drug Delivery Rev.*, 2009, **61**, 478–486.
- R. M. Devendiran, S. K. Chinnaiyan, N. K. Yadav, G. K. Moorthy, G. Ramanathan, S. Singaravelu, U. T. Sivagnanam and P. T. Perumal, *RSC Adv.*, 2016, **6**, 29757–29768.

- 44 R. M. Devendiran, S. K. Chinnaiyan, N. K. Yadav, G. Ramanathan, S. Singaravelu, P. T. Perumal and U. T. Sivagnanam, *RSC Adv.*, 2016, **6**, 32560–32571.
- 45 X. S. Zhu, L. Zhu, Z. H. Duan, R. Q. Qi, Y. Li and Y. P. Lang, *J. Environ. Sci. Health, Part A: Toxic/Hazard. Subst. Environ. Eng.*, 2008, **43**, 278–284.
- 46 J. Dhanapal, M. Ravindran and S. Baskar, *Anti-Cancer Agents Med. Chem.*, 2015, **15**, 248–257.
- 47 C. L. Xu, L. D. Cao, P. Y. Zhao, Z. L. Zhou, C. Cao, F. Zhu, F. M. Li and Q. L. Huang, *Int. J. Mol. Sci.*, 2018, **19**, 854.
- 48 F. F. Liu, Y. R. Long, Q. X. Zhao, X. Liu, G. R. Qiu, L. Zhang, Q. J. Ling and H. B. Gu, *Polymer*, 2018, **143**, 212–227.
- 49 OECD Validation Report (Phase 1) for the Zebrafish Embryo Toxicity Test: Part I and Part II. Series on Testing and Assessment No. 2011, 157, OECD, Paris.
- 50 G. R. Qiu, L. Zhao, X. Liu, Q. X. Zhao, F. F. Liu, Y. Liu, Y. W. Liu and H. B. Gu, *React. Funct. Polym.*, 2018, **128**, 1–15.
- 51 Z. Q. Cao and G. J. Wang, *Chem. Rec.*, 2016, **16**, 1398–1435.
- 52 X. Wu, L. Gao, X. Y. Hu and L. Wang, *Chem. Rec.*, 2016, **16**, 1216–1227.
- 53 Z. X. Lin, S. H. Liu, W. T. Mao, H. Tian, N. Wang, N. H. Zhang, F. Tian, L. Han, X. L. Feng and Y. Y. Mai, *Angew. Chem., Int. Ed.*, 2017, **56**, 7135–7140.
- 54 D. Xiong, G. Liu, L. Hong and E. Duncan, *Chem. Mater.*, 2011, **23**, 4357–4366.
- 55 K. Qi, Q. G. Ma, E. E. Remsen, C. G. Clark and K. L. Wooley Jr., *J. Am. Chem. Soc.*, 2004, **126**, 6599–6607.
- 56 F. Xu, H. Li, Y. L. Luo and W. Tang, *ACS Appl. Mater. Interfaces*, 2017, **9**, 5181.
- 57 Y. L. Hu, W. Qi, F. Han, J. Z. Shao and J. Q. Gao, *Int. J. Nanomed.*, 2011, **6**, 3351–3359.
- 58 X. Liu, S. D. Mu, G. R. Qiu, Y. R. Long, Q. J. Ling, J. J. He and H. B. Gu, *Polymer*, 2018, **146**, 275–290.